

Street environment change detection from mobile laser scanning point clouds



Wen Xiao*, Bruno Vallet, Mathieu Brédif, Nicolas Paparoditis

Université Paris-Est, IGN, Lab MATHIS, 73 Av. de Paris, 94160 Saint-Mandé, France

ARTICLE INFO

Article history:

Received 22 December 2014

Received in revised form 2 April 2015

Accepted 22 April 2015

Available online 11 May 2015

Keywords:

Change detection

Lidar

K-d tree

Occupancy grids

Point-to-triangle distance

Dempster–Shafer theory

ABSTRACT

Mobile laser scanning (MLS) has become a popular technique for road inventory, building modelling, infrastructure management, mobility assessment, etc. Meanwhile, due to the high mobility of MLS systems, it is easy to revisit interested areas. However, change detection using MLS data of street environment has seldom been studied. In this paper, an approach that combines occupancy grids and a distance-based method for change detection from MLS point clouds is proposed. Unlike conventional occupancy grids, our occupancy-based method models space based on scanning rays and local point distributions in 3D without voxelization. A local cylindrical reference frame is presented for the interpolation of occupancy between rays according to the scanning geometry. The Dempster–Shafer theory (DST) is utilized for both intra-data evidence fusion and inter-data consistency assessment. Occupancy of reference point cloud is fused at the location of target points and then the consistency is evaluated directly on the points. A point-to-triangle (PTT) distance-based method is combined to improve the occupancy-based method. Because it is robust to penetrable objects, e.g. vegetation, which cause self-conflicts when modelling occupancy. The combined method tackles irregular point density and occlusion problems, also eliminates false detections on penetrable objects.

© 2015 International Society for Photogrammetry and Remote Sensing, Inc. (ISPRS). Published by Elsevier B.V. All rights reserved.

1. Introduction

Change detection techniques have been applied in different fields such as environment monitoring (Tian et al., 2013), 3D city model updating (Taneja et al., 2013), street environment inventory (Pu et al., 2011), simultaneous localization and mapping (SLAM) (Wolf and Sukhatme, 2004; Moras et al., 2011), moving object tracking (Yin and Collins, 2007; Irani and Anandan, 1998; Lindstrom and Eklundh, 2001), surveillance systems (O'Callaghan and Haga, 2007) and so on. The spatial scale can be as large as a whole country, a forest, a city or as small as a street. Objects of interest vary from ground surfaces, vegetation, buildings, cars to pedestrians.

In remote sensing studies, large coverage images are usually used for large spatial scale change detection in forest or urban areas for land-cover and land-use monitoring (Hussain et al., 2013; Tian et al., 2013). Airborne laser scanning (ALS) data is also used for similar applications with high geometric precision due

to accurate 3D acquisition (Xu et al., 2013; Hebel et al., 2013; Yu et al., 2004). In recent years, 3D maps and virtual city models have been under fast development, therefore many studies have focused on street environment monitoring and city model updating (Früh and Zakhor, 2004; Kang et al., 2013).

Mobile mapping systems (MMSs) can easily scan streets multiple times, therefore allow us to detect changes at street or even city-scale. A MMS is often a georeferenced vehicle mounted with image and/or laser sensor used for environment mapping. Laser scanning provides precise 3D geometric information on the environment, which is of great interest for 3D mapping, localization, scene perception, motion tracking and navigation purposes. Studies from computer vision mainly use imagery for city and street scene change detection (Pollard and Mundy, 2007; Sakurada et al., 2013; Košecka, 2013; Eden and Cooper, 2008; Taneja et al., 2011, 2013). However, lidar (light detection and ranging) data (also referred to as laser scanning data, range data or lidar point clouds) have been proven to be an accurate data source for 3D urban reconstruction (Lafarge and Mallet, 2011; Chauve et al., 2010; Verma et al., 2006; Zhou and Neumann, 2010; Toshev et al., 2010; Banno et al., 2008; Poullis, 2013), infrastructure management and road inventory (Pu et al., 2011; Zhou and

* Corresponding author. Tel.: +33 143988000 + 7643.

E-mail addresses: wen.xiao@ign.fr (W. Xiao), bruno.vallet@ign.fr (B. Vallet), bruno.vallet@ign.fr (M. Brédif), nicolas.paparoditis@ign.fr (N. Paparoditis).

URL: <http://recherche.ign.fr/labos/matis/~xiao> (W. Xiao).

Vosselman, 2012). Thus, mobile laser scanning (MLS) data is intensively studied nowadays (Weinmann et al., 2014; Demantké et al., 2011; Monnier et al., 2012; Yang and Dong, 2013; Aijazi et al., 2013; Serna and Marcotegui, 2014; Qin and Gruen, 2014).

Change detection methods specific to MLS point clouds have been seldom investigated, therefore the development of corresponding approaches becomes urgent. State-of-the-art distance-based methods, e.g. point-to-point, point-to-plane or point-set to point-set distances, may be used for this purpose (Girardeau-Montaut et al., 2005). However, irregular point density and occlusions still remain major challenges. In this paper, we aim to develop a street environment change detection method that is robust to point density variations and capable of distinguishing occlusions from real changes. First, related work and our contribution are discussed in Section 2. Then, the concept of occupancy-based change detection is explained in Section 3. Section 4 presents the PTT distance-based method and the combination with the occupancy-based one. Section 5 describes the experiments and the corresponding results. Quantitative evaluation is demonstrated in Section 6. Finally, conclusions are drawn and limitations are discussed in Section 7.

2. Related work

Change detection has been studied in different fields, e.g. remote sensing and photogrammetry, computer vision, robotics. Related work is presented based on different approaches.

2.1. Change detection from remote sensing and airborne lidar data

Remote sensing change detection approaches vary from pixel-based, region-based to object-based methods. Hussain et al. (2013) summarize approaches as pixel-based, e.g. image differencing, and object-based, e.g. classified object comparison, for remotely sensed images. Tian et al. (2013) use a region-based method for building and forest change detection, and claim that region-based methods perform generally better than pixel-based methods. Similarly, change detection using airborne laser scanning (ALS) data also starts from pixel-based method. Murakami et al. (1999) subtract digital surface models (DSMs) generated from ALS data at different times. Then a simple shrinking and expansion filter was utilized to remove edges of unchanged features. Changes are detected by simple image differencing at 2.5D. Many later studies follow the same strategy for both urban and forest environment change detection (Steinle and Bahr, 2003; Matikainen et al., 2003; Vögtle and Steinle, 2004; Yu et al., 2004; Champion et al., 2009; Choi et al., 2009; Rutzinger et al., 2010). Walter (2004) uses pixel-based and object-based classification of multispectral and lidar data for change detection in geographic information system (GIS) databases. Vosselman et al. (2004) classify ALS data as bare-earth, building and vegetation, and then compare with a topographical database for map updating. Xu et al. (2013) detect and classify changes in buildings after classification of ALS data into urban objects.

2.2. Change detection from terrestrial and mobile lidar data

Terrestrial laser scanning (TLS) and MLS data demand more accurate detection methods. Object-based change detection can be affected by the object recognition accuracy, thus point-based and region-based methods are often used. Girardeau-Montaut et al. (2005) propose a framework to detect changes from terrestrial lidar data semi-automatically. Point clouds are directly compared using three methods, i.e. average distance, best fitting plane orientation and the Hausdorff distance (the maximum

distance among the points in one set to the closest point in another set). Results show that the Hausdorff distance performs best. A local model for distance calculation is suggested in order to avoid density variation issues. Kang et al. (2013) also use the Hausdorff distance to detect changes in buildings from TLS data. Point-to-point distance-based methods are practical for TLS and MLS data because changes can be detected directly in 3D. Nevertheless, point-to-point distance is very sensitive to point density. A local surface model can be helpful, since for example point-to-triangle distance (PTTD) or point-to-plane distance are more robust than single point-to-point distances. Zeibak and Filin (2007) treat 3D laser scans as range panoramas. Range images are compared from the sensor perspective, which avoids false detection on occluded parts. Qin and Gruen (2014) detect changes at street level using MLS point clouds and terrestrial images. After co-registration, points are projected onto each image. Then, stereo pairs of terrestrial images are compared with point clouds to find the geometrical consistency. Finally, initial changed areas are optimized by graph cut. Aijazi et al. (2013) firstly classify MLS data into permanent and temporary classes, and then construct similarity maps on the 3D voxels for multiple epoch data fusion to build a complete 3D urban map.

2.3. Change detection in computer vision

3D change detection has been applied to moving object detection and urban environment monitoring in computer vision. Yin and Collins (2007) detect moving objects by a Belief Propagation approach using a 3D Markov Random Field (MRF). A similar method has been presented by Koščeká (2013) to detect changes from street scene images. Changes are differentiated as structural, appearance change or temporary dynamically moving objects. Sakurada et al. (2013) detected changes of 3D urban structures from a vehicle-mounted camera. The similarity of the local image patches is computed from multi-view images. The method is compared with Multi-View Stereo (MVS) based methods. Many investigations are based on voxelized space, which performs better than MVS models as compared by Taneja et al. (2011). Structural changes have been detected by voxelizing places of interest. Geometric consistencies between voxels are evaluated. Inconsistency indicates a change in the scene. They extend the work to city-scale in order to detect changes in cadastral 3D models for facilitating the model updating process (Taneja et al., 2013). Pollard and Mundy (2007) store probability distributions for surface occupancy and image appearance in 3D voxel grids. Then they are updated by new images based on Bayesian decision theory. The changes are detected by thresholding the probability to obtain a binary mask. The work has been extended to 4D by Ulusoy and Mundy (2014). 3D changes are detected on 3D models in a time series for model updating instead of rebuilding models at each time.

2.4. Change detection using occupancy grids from robotics

Pagac et al. (1996) use occupancy grids for constructing and maintaining a map of an autonomous vehicle's environment for navigation purposes. A sensor beam is projected on a rectangular grid assigned probabilities of cells being empty, full and ignorance outside the beam. Every cell is initialized, $m(\text{empty}) = m(\text{full}) = 0$ and $m(\text{ignorance}) = 1$, then the Dempster-Shafer Theory (DST) is used to fuse the sensor readings. The DST has proved to outperform the Bayesian method which needs to specify all conditional probabilities even if no *a priori* information exists. Wolf and Sukhatme (2004) also use an occupancy grid for SLAM in dynamic environments. The states of the occupancy grid are defined as *Free*, *Unknown* and *Occupied*. Two different grids are used to model

static and dynamic parts of the environment and then combined. The algorithm is capable of detecting dynamic objects in the environment. Most of the previous studies model occupancy in 2D grid cells. Underwood et al. (2013) detect changes in 3D from Lidar data using ray tracing which is similar to occupancy modelling. Changes are categorized as *additions*, *subtractions* and *discrepancies* w.r.t. the previous occupancy state. A spherical reference frame is proposed to present the relative position of two scans. Laser beams are treated as cone-shaped. Then changes are detected by setting thresholds on range distances. Hebel et al. (2013) detect changes in airborne laser scanning (ALS) point clouds using voxel indexing. The occupancy of laser rays is modelled by sigmoid functions. Then the DST is applied to combine multiple measurements. Vegetation is modelled with different parameters from others due to self-conflicting. Changes in buildings and cars are successfully detected. However, data acquisition and registration accuracies have not been considered.

Our preliminary occupancy-based method has shown the capability and reliability of urban environment change detection at object level (Xiao et al., 2013). Urban objects, e.g. cars, garbage bins, bicycles, pedestrians, were successfully detected in the conducted experiments. However, the datasets were small, field of view was narrow (only lower part of the street, no vegetation scanned), and objects were close to the sensor. Most importantly, occupancy around the point was simply modelled along the ray direction, which leads to misdetections (details in Section 3.1). In this paper, we present the improved method of occupancy modelling around a ray and, especially, around the point considering its normal. Moreover, we utilize completely new challenging datasets, which cover a large area in a complex street environment without human intervention, and have massive number of points and irregular point density. In addition, we combine the occupancy-based method with a PTT distance-based method, which is robust to penetrable objects, to further improve the change detection result. Statistical analysis and comparison are also conducted.

Compared to related work, our main contribution is a method that is robust to irregular point density and able to distinguish occlusions from real changes in MLS data. In more detail:

- **Combination of occupancy and distance:** Occupancy-based method is able to distinguish occlusions from real changes, and distance-based method is robust to penetrable objects. They are complementary to each other. We take the advantages of both to improve the final change detection result.
- **Local cylindrical reference frame:** A local cylindrical reference frame is defined from the sensor's perspective according to the scanning geometry to interpolate evidence when it is missing between rays.
- **K-d tree for point query:** The scope of a scan ray is not considered as a cone but a prism. A K-d tree is used to optimize the query of points inside the prism.
- **No voxelization:** Consistency is evaluated directly on points without voxelization. We demonstrate that conflicts (changes) may only occur near the points at one of the compared epoch data. Thus, evidence is accumulated directly at points' locations to compare with the other epoch.
- **Occupancy modelling considering uncertainties:** Occupancy states are modelled elaborately over a scan ray and around the point in 3D with physical meanings, taking into account the acquisition geometry and the underlying uncertainties.
- **Point-to-triangle distance (PTTD):** Due to the inconsistent point density and the complexity of street objects, we propose PTTD instead of point-to-point or point-to-plane distances. The Delaunay triangulation moderately generalizes the object surfaces.

3. Occupancy-based change detection

The principle of our occupancy-based approach is that a laser scan ray indicates the occupancy of space. Scenes covered by laser scans can be represented by such occupancy. If scenes have changed, the occupancy of space will change as a result. The inconsistency of occupancies between datasets will then indicate the changes.

The workflow including three main steps is illustrated in Fig. 1. Two epoch data are taken for comparison, one target, one reference. To obtain the change information of the target points, first, occupancy of a single ray from the reference data is modelled, considering the measurement and registration uncertainties. Then, occupancies of all the rays from the reference data are fused together. Last, the occupancy of the reference space is compared with the occupancy of each target points resulting in the consistency between these two. Then changes are detected based on the consistency assessment (details in Section 3.3). The workflow depicts the detection of changes in the target data w.r.t. the reference data, whereas the two datasets are exchangeable since the method is symmetrical.

3.1. Occupancy modelling for an individual ray

This section firstly presents the DST and its application to occupancy modelling, following which the improved modelling method is presented. Then, uncertainties are integrated with the occupancy functions.

3.1.1. Occupancy modelling along a ray

One advantage of the DST is that the combination rule is commutative and associative so that evidence can be fused in any order, which is essential for handling objects scanned from different perspectives and datasets acquired at different times. It allows to combine evidence from different sources and arrive at a degree of belief representing all possible states of a system. The state of space occupancy can be *empty* or *occupied*, represented by a universal set $X = \{\text{empty}, \text{occupied}\}$. The power set of X , $2^X = \{\emptyset, \{\text{empty}\}, \{\text{occupied}\}, \{\text{empty}, \text{occupied}\}\}$, contains all of its subsets. Due to occlusions in data acquisition, no information is obtained in shadow areas; hence, the occupancy state is unknown. When the occupancy of space is *unknown*, it can be either *empty* or *occupied*, so the set $\{\text{empty}, \text{occupied}\}$ represents state *unknown*. According to the DST, the mass (m) of each element of the power set is within the range $[0, 1]$. Moreover, the mass of the empty

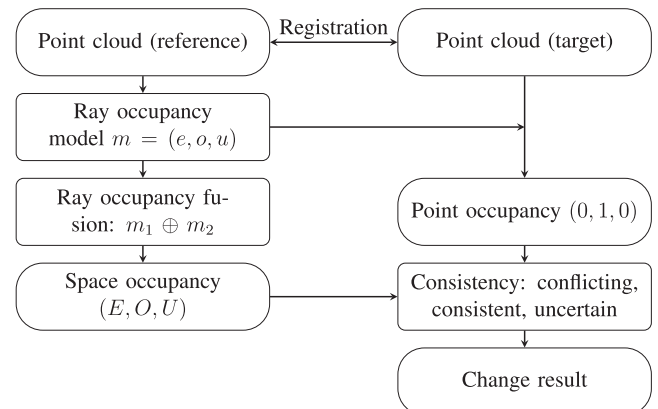


Fig. 1. Flowchart of our occupancy-based method including three main steps: single ray occupancy modelling, ray occupancy fusion in reference data, and consistency assessment between reference and target point clouds.

set is 0 and the masses of the remaining subsets add up to a total of 1:

$$m : 2^X \rightarrow [0, 1], m(\emptyset) = 0, \sum_{A \in 2^X} m(A) = 1 \quad (1)$$

The DST represents all the three states of occupancy and sets a range for each state. This avoids the effect of redundancy due to repetitive scanning. The mass of each state, $m\{\text{empty}\}$, $m\{\text{occupied}\}$ and $m\{\text{unknown}\}$ are abbreviated as e, o and u respectively.

For a laser scanning ray, occupancy along the ray is defined as: *empty* between a laser point and its scanning origin, so $e_r = 1$, $o_r = 0$; *occupied* at the location of the point, $e_r = 0$, $o_r = 1$; *unknown* behind the point. The mass of occupancy is represented by a Gaussian function. o_r decreases from 1 to 0, and u_r increases from 0 to 1 accordingly (Fig. 2).

A laser ray is not a perfect line but a cone-shaped beam with a particular footprint. The occupancy around the ray can be parametrised by the angle of the cone. A simple cone-shaped ray is given in Fig. 3. Due to uncertainties, the edge of the laser beam is fuzzy.

In reality, point clouds, unlike images, do not cover the whole scanned space. There are gaps between rays. And the gaps vary due to many factors, e.g. vehicle speed, object distance and incidence angle. A simple cone shape will not cover the gaps, therefore will induce under-detection. One single parameter of the ray (angle of the cone) is not sufficient for occupancy interpolation.

3.1.2. Improved occupancy modelling around a point

A common MMS configuration (Paparoditis et al., 2012) is scanning the profile of surroundings with a laser scanner rotating vertically to the vehicle trajectory. A local reference frame (Fig. 4) is presented to define the occupancy around rays to interpolate the gaps between rays. The origin O is the sensor center, θ represents the vertical rotating angle, and t is the distance in the trajectory direction. Together with the distance in the ray \overrightarrow{OP} direction r , θ and t define the occupancy around the ray in a local cylindrical coordinate system.

In the ray direction, occupancy was previously simply defined as in Fig. 2 (Xiao et al., 2013). However, the default assumption is that point normals are always in the same direction as the rays, which is obviously false in reality. As shown in Fig. 5a, the green point is behind the red one in the ray direction, then it will be considered as located in the *unknown* part of the ray. However, they are actually on the same surface. This happens when the incidence angle is large.

To overcome this issue, we improve the method by considering the normal directions of points and modelling occupancy around the surface (Fig. 5b). Occupancy is modelled as: *empty* between the origin of a point and its surface ($e_n = 1$); *occupied* around the surface ($o_n = e^{-\frac{1}{2}(\frac{r}{\lambda_n})^2}$); and *unknown* behind the surface ($u_n = 1 - o_n$). λ_n represents the mass of occupancy in the normal

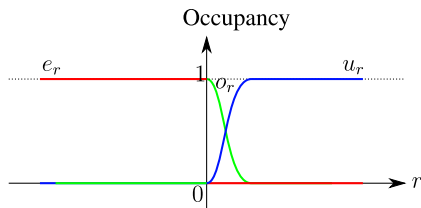


Fig. 2. Occupancy in the ray direction: *empty* between a laser point and its scanning origin; *occupied* at the location of the point; *unknown* behind the point (Origin is the point location, r represents the distance to the point in the ray direction).

direction and behind the surface of the modelled object. Occupancy on the surface along the scan line direction is modelled by a Gaussian function $f_s = e^{-\frac{1}{2}(\frac{s}{\lambda_s})^2}$, ranging from 0 to 1. And $\lambda_s = r \cdot \lambda_o / \cos \beta$, r is the distance between a point and its origin in the ray direction, β is the angle between the ray and the point normal, λ_o represents the angular mass of occupancy on the sensor rotating plane.

Now the occupancy has been modelled for the ray and angular directions, which are transformed onto the point normal direction and scan line direction on the corresponding surface. Theoretically, the occupancy masses in the rotating direction should be the same as in the trajectory direction since the ray is cone-shaped. However, sampling densities are not the same in these two directions. The horizontal sampling depends on the vehicle speed while the vertical density depends on the object distance and the incidence angle. To overcome this anisotropic sampling, these two directions are considered independently to interpolate the gaps. Thus, in the trajectory direction t , the mass of occupancy is

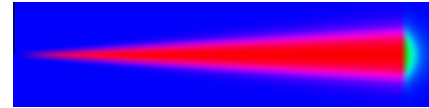


Fig. 3. Cone-shaped laser beam (red: empty, green: occupied, blue: unknown). (For interpretation of the references to color in this figure legend, the reader is referred to the web version of this article.)

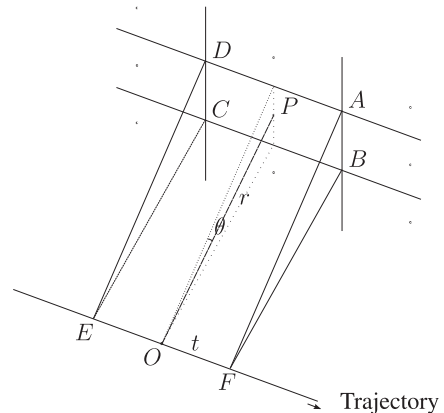


Fig. 4. Cylindrical local reference frame for occupancy modelling around a ray OP and its triangular prism shaped vicinity $ABCD-EF$.

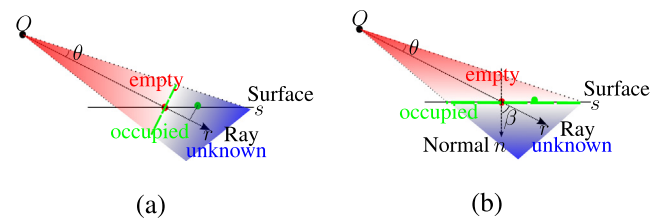


Fig. 5. Occupancy around a point (red: empty, green: occupied, blue: unknown). If occupancy is modelled along the ray (a), the green point will be considered in the shadow of the red one since it falls behind in the ray direction r . However, in reality, they are on the same surface s , so occupancy is modelled along the point normal n (b). (For interpretation of the references to color in this figure legend, the reader is referred to the web version of this article.)

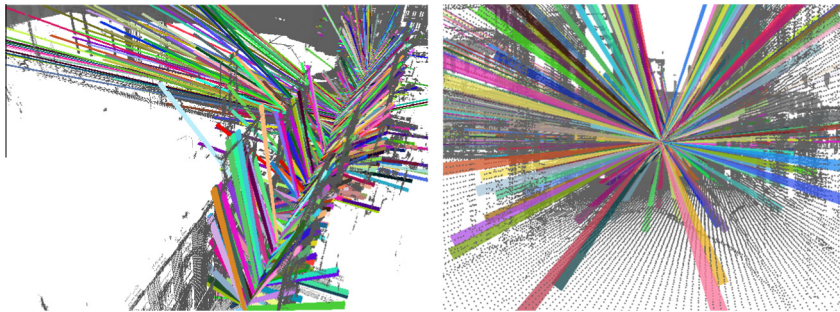


Fig. 6. Corresponding point search with prism-shaped rays using K -d tree (points in gray, sub-sampled rays in random colors): (left) perspective view and (right) view along trajectory. (For interpretation of the references to color in this figure legend, the reader is referred to the web version of this article.)

modelled as $f_t = e^{-\frac{1}{2}(\frac{t}{\lambda_t})^2}$. The value of λ_t depends on the gap between scan lines.

When it is far from a ray, there will be no mass contributing by this ray, namely a ray only has mass in its vicinity (defined as 3 times λ_0 , λ_t and λ_r). The vicinity is a triangular prism $ABCD-EF$ according to the cylindrical reference frame (Fig. 4). Occupancy mass out of the prism is significantly small hence can be neglected. The prism is used for K -d tree corresponding point searching (details in Section 3.2). The local reference frame is defined for a specific MMS configuration, however it is adaptable as long as the whole space is covered. The idea is to interpolate the space from the sensor's perspective.

3.1.3. Uncertainty modelling

Uncertainties of measurement (ranging) and registration are taken into consideration since they can induce changes at fine scales. Both of them are represented by normal distributions with standard deviations σ_m and σ_r . Since the three directions, n , s , t are pairwise perpendicular, uncertainties are considered separately in each direction. In the normal direction, the error of measurement has partial effects since the ranging measurement error only exists in the ray direction. Thus, the overall uncertainty σ_n is the combination of the registration error and the projection of measurement error. They are taken into account by convolving the two error distributions, resulting in a Gaussian function F_n with standard deviation $\sigma_n = \sqrt{\sigma_r^2 + (\sigma_m \cdot \cos\beta)^2}$. Similarly, perpendicular to the normal, the uncertainty on the surface σ_s is modelled as a Gaussian function F_s with standard deviation $\sigma_s = \sqrt{\sigma_r^2 + (\sigma_m \cdot \sin\beta)^2}$. Since in the trajectory direction, measurement error does not exist, the uncertainty only comes from the error of registration, therefore $\sigma_t = \sigma_r$ for the uncertainty function F_t .

Uncertainties are taken into account by convolving with occupancy functions. In the normal direction, three occupancy states are convolved individually with the uncertainty function:

$$e'_n = e_n \otimes F_n; \quad o'_n = o_n \otimes F_n; \quad u'_n = u_n \otimes F_n = 1 - e'_n - o'_n \quad (2)$$

And in the other two directions, occupancy functions after convolution are:

$$f'_s = f_s \otimes F_s; \quad f'_t = f_t \otimes F_t \quad (3)$$

The overall occupancy of ray \overrightarrow{OP} is a function of parameters $n, s, t : n$ defines the state of occupancy and also the value of each state; s and t interpolate the occupancy around the ray. The occupancies in s and t directions drop from 1 to 0 when values of s and t

increase. They can be considered as weights of the occupancy states in the normal direction. Thus they are multiplied with occupancy state functions as follows:

$$m(\overrightarrow{OP}) = \begin{cases} e \\ o \\ u \end{cases} = \begin{cases} e'_n \cdot f'_s \cdot f'_t \\ o'_n \cdot f'_s \cdot f'_t \\ 1 - e - o \end{cases} \quad (4)$$

3.2. Occupancy fusion and corresponding point retrieval

After modelling occupancy for each single ray, the occupancy of a whole epoch data can be obtained by combining occupancies of all the rays from the epoch, which can then be compared with the target data. In practice, we first search the corresponding target points using the prism-shaped ray scope. Then the occupancy is modelled directly at the location of each point. A point can be within the scope of multiple rays, whose occupancies are then fused to compare with the point's occupancy.

3.2.1. Corresponding point retrieval

For each ray in the reference data, a prism is built according to the local cylindrical frame. It is then used to retrieve the points that are inside the scope of this ray. The problem is to query a K -d tree of 3D points, which is built on the target point cloud, with a convex polyhedron (prism) (Fig. 6). The bounding box (BBox) of each non-leaf cell of the K -d tree is checked whether it intersects with the prism. In 3D, it is the intersection between two convex polyhedra: a cell BBox B and a prism P . They do not intersect when there exists a separating plane lying in between which is (i) parallel to a face of B , (ii) parallel to a face of P , or (iii) parallel to an edge of B and an edge of P (Greene, 1994).

Separating planes in the three cases are estimated: (i) plane separation supported by a face of B amounts to testing if all the vertices $p \in P$ are on the same side of the face. In fact, only the nearest vertex to the face is necessary to be verified. Here, the nearest vertex means the one with the smallest coordinates w.r.t. the face normal. The nearest vertex $p_N \in P$ for each face of B is tested; (ii) similarly, for each face of P , the normal direction and the face plane are constructed. And the nearest vertex $b_N \in B$ is checked whether it crosses the plane; (iii) separating planes are constructed by an edge of B and an edge of P . For each edge $E_P \in P$, three planes that are passing through E_P and parallel to the three axes of B are constructed. Then the nearest vertex $b_N \in B$ for each of the three planes is checked whether it is on the same side as P . In any of the cases, if the nearest vertex does not cross the separating plane, B and P do not intersect with each other.

To gather points of the K -d tree contained in the query prism, the K -d tree is traversed from the root by pruning sub-trees whose BBoxes do not intersect with P . Finally, a

point-in-convex-polyhedron test is performed on all the points of the traversed K-d tree nodes to filter the exact list of points inside P . Based on test performances, approximate point query without case (iii) is even more computationally efficient because case (iii) is rather complex. It is the trade-off between pruning more sub-trees and conducting more *point-in-convex-polyhedron* tests. For each point inside the prism, the occupancy at the location of this point is then modelled according to the ray in the local reference frame.

3.2.2. Occupancy fusion

A target point can be inside of multiple ray prisms, each of which contributes its own occupancy. Thus the overall occupancy at the point location needs to be fused. Occupancy is fused by the DST. Dempster's rule of combination is as follows:

$$m_{1,2}(A) = (m_1 \oplus m_2)(A) = \frac{1}{1-K} \sum_{B \cap C = A \neq \emptyset} (m_1(B) \cdot m_2(C)) \quad (5)$$

where $B \in 2^X$, $C \in 2^X$ and K is the conflict between two mass sets:

$$K = \sum_{B \cap C = \emptyset} (m_1(B) \cdot m_2(C)) \quad (6)$$

In our case, $\{e\}$ and $\{o\}$ are the subsets of $\{u\}$ because space can be both *empty* or *occupied* when the state is *unknown*. The combined occupancy of two rays $m_1 \oplus m_2$ is:

$$m_1 \oplus m_2 = \left\{ \begin{array}{l} e_1 \\ o_1 \\ u_1 \end{array} \right\} \oplus \left\{ \begin{array}{l} e_2 \\ o_2 \\ u_2 \end{array} \right\} = \frac{1}{1-K} \left\{ \begin{array}{l} e_1 \cdot e_2 + e_1 \cdot u_2 + u_1 \cdot e_2 \\ o_1 \cdot o_2 + o_1 \cdot u_2 + u_1 \cdot o_2 \\ u_1 \cdot u_2 \end{array} \right\} \quad (7)$$

in which $K = o_1 \cdot e_2 + e_1 \cdot o_2$. The combination rule is commutative and associative, so the order of combination is arbitrary.

Then for a given reference point P , which lies inside the scope of I rays $R_i (i \in I)$, the overall occupancy at this location is updated by combining all the rays' occupancies:

$$m(P) = \bigoplus_{i \in I} m(R_i) \quad (8)$$

Due to large amount of data, Lidar point clouds are usually cut into small blocks and stored separately in different files. One object can be scanned from different perspectives, therefore points from the same object will be stored in several files. Since Dempster's rule is associative, we can process any file in any order. The K-d tree keeps the processing time at a relatively low level (tens of minutes instead of hours).

3.3. Consistency assessment between different epochs

To detect the changes between two epoch data, we define consistency relations between their occupancies. They are *conflicting* when one is *empty* whereas the other one is *occupied* or vice versa, *consistent* when they have the same occupancy state, and *uncertain* if one is *unknown* whereas the other is known. The consistency relations between two datasets, target (E_1, O_1, U_1) and reference (E_2, O_2, U_2) , are defined as:

$$\begin{aligned} \text{Conflicting} &= E_1 \cdot O_2 + O_1 \cdot E_2 \\ \text{Consistent} &= E_1 \cdot E_2 + O_1 \cdot O_2 + U_1 \cdot U_2 \\ \text{Uncertain} &= U_1 \cdot (E_2 + O_2) + U_2 \cdot (E_1 + O_1) \end{aligned} \quad (9)$$

To compute the consistency relations, one simple method is to voxelize space, compute the occupancy of each dataset on each voxel using the same size, and then compare the occupancy values of two registered datasets on every voxel. This method provides a consistency result on the whole scene at once. However, it is

computationally expensive. There is no need to compute the occupancy over the whole space since we are interested in changes (conflicts) which, based on its definition (Eq. (9)), only occur at places that are empty at one epoch and occupied at another. A point gives the evidence that the space is occupied. So to know if the point has changed or not, we only need to compute consistency at the location of this point. The result of our algorithm is therefore the consistency information (*consistent*, *conflicting*, *uncertain*) of each point, which is more straightforward than representing this information on a voxel grid. An occupancy voxel grid will only be useful when the scene is scanned a high number of times when the number of acquired points becomes higher than the number of voxels required to model the scene with sufficient resolution.

According to Section 3.1, the occupancy at a target point is $m(P) = (e_1, o_1, u_1) = (0, 1, 0)$. After considering uncertainties, the maximum *occupied* value shifts slightly behind to P_s , $m(P_s) = e'_1, o'_1, u'_1 \simeq (0, 1, 0)$ (Xiao et al., 2013). Then to obtain the consistency information of this point, we need to compare it with the occupancy of the reference dataset at P_s , which is the combination of occupancies of neighboring rays. The consistency relations at P_s are as follows:

$$\begin{aligned} \text{Conf}(P_s) &= e'_1 \cdot O_2 + o'_1 \cdot E_2 \simeq E_2 \\ \text{Cons}(P_s) &= e'_1 \cdot E_2 + o'_1 \cdot O_2 + u'_1 \cdot U_2 \simeq O_2 \\ \text{Unce}(P_s) &= u'_1 \cdot (E_2 + O_2) + U_2 \cdot (e'_1 + o'_1) \simeq U_2 \end{aligned} \quad (10)$$

If the location at P_s is empty in the reference data, then it conflicts with the occupancy of the target point, which indicates a change. If the location is also occupied, it is consistent, i.e., there is no change. If the location is unknown, it means that either the point is in the shadow or there are no counterparts in the reference data, thus it is uncertain whether it has changed or not.

4. Combination with a point-to-triangle distance-based change detection

Occupancy-based approach may detect false changes on objects that are penetrable, e.g. trees, fences, because rays can pass through them, meaning the space around them is empty. Thus points on these objects will conflict with rays that travelled through. Hebel et al. (2013) treat this situation separately using different parameters for vegetation which is pre-classified automatically. In our case, we have no *a priori* class information on the data.

Conventional point-to-point distance-based methods may avoid this failure because neighboring points can be found for points on these objects from another epoch if the distance threshold is large enough. Direct point-to-point comparison suffers from irregular point density. To minimize the effect of anisotropy, a local surface model or a small point cluster is recommended (Girardeau-Montaut et al., 2005). However the size or the number of points for the model can be tricky to chose. Due to the complexity of street objects, we use the point-to-triangle distance.

Distance to the nearest triangle in the reference data is computed instead of the nearest point. A certain number of nearest points are retrieved first from the reference data, then a local Delaunay triangulation is implemented on these points. The number of points is not vital because we only look for the nearest triangle, which should not be different as long as the number is not too small. Afterwards, the nearest triangle is found considering the distance from the target point to each triangle in 3D. If the target point projects inside the triangle, the distance to the projection is the PTTD. If the projection is outside the triangle, the distance to the nearest edge of the triangle is considered as the PTTD (Fig. 7). Then points that are changed are detected by thresholding the minimum distance (d_{min}).

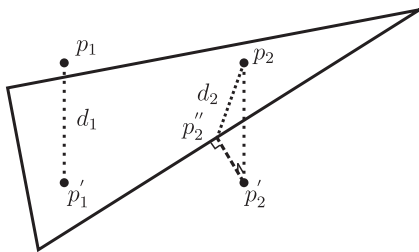


Fig. 7. Point-to-triangle distance (PTTD) in 3D: if the projection is inside the triangle as p_1' , the projection distance is the PTTD, $d_1 = p_1 p_1'$; whereas if it is outside as p_2' , the distance to the nearest edge of the triangle is considered as the PTTD, $d_2 = p_2 p_2''$.

Table 1
Summary of notation definitions and parameter settings.

Notations	Definitions and settings
Occupancy notations	
(e, o, u)	Abbreviations of the masses (empty, occupied, unknown)
(e_n, o_n, u_n)	(e, o, u) in the normal direction
(e', o', u')	(e, o, u) after convolving with uncertainty functions
f_n, f_s, f_t	Occupancy function in normal, scan line and trajectory directions
(E, O, U)	(empty, occupied, unknown) for a whole epoch data after fusion
Geometric notations	
r, θ, t	Local reference frame of ray, angular and trajectory directions
n, s, β	Local geometry between ray and point normal (Fig. 5b)
Data features	
σ_m, σ_r	Variance of measurement and registration
$\sigma_n, \sigma_s, \sigma_t$	Variance of uncertainty in each direction
Physical parameters	
λ_s	Occupancy in scan line direction $\lambda_s = r \cdot \lambda_\theta / \cos \beta$
Tunable parameters	
λ_n	Occupancy in n direction, thickness of urban objects (0.3 m)
λ_θ	Occupancy in θ direction, half of the angular resolution
λ_t	Occupancy in t direction, covers gaps between scan lines (0.1 m)

$$m(P) = \begin{cases} 1 & \text{if } \text{PTTD} < d_{\min}, \\ \oplus_{i \in I} m(R_i) & \text{else.} \end{cases} \quad (11)$$

The occupancy-based and PTTD-based methods are integrated as shown in Eq. (11). If a point has nearby corresponding triangles ($\text{PTTD} < d_{\min}$), the occupancy at its location is set to be 1. Otherwise, the occupancy is the fusion of neighboring rays' occupancies according to Eq. (8). Points that are changed should be far from other points as well as be *conflicting* with neighboring rays.

5. Experiments and result

Two experimental data at different sites were acquired in Paris by a MMS called *Stereopolis* (Paparoditis et al., 2012) using two RIEGL laser scanners, LMS-Q120 and VQ-450. Both rotate perpendicularly to the vehicle trajectory, scanning profiles of the street environment. One has only 80° vertical field of view (FOV) (data referred to as Data 1), whereas the other scans a full circle (360° FOV) (Data 2). Each site has two epoch data. Datasets are registered by the method proposed by Monnier et al. (2013) with about 0.1 m accuracy using non-rigid iterative closest point (ICP). Point normals are estimated by the method from Demantké et al. (2011) in which the optimal spherical neighborhood is automatically defined. Three dimensionality (linear, planar, volumetric) features are computed at multiple radius scales. Then the best radius is automatically selected when one feature is mostly dominant over the two others. Point normals are given by the principle component analysis (PCA) on the optimal neighborhood.

Many variables and parameters have been defined in previous sections, Table 1 summarizes the definition of notations and parameter settings. Parameters are set according to the scanning geometry. The scan ray rotates perpendicularly to the vehicle trajectory. Rotation angle and sensor origin are recorded for each point. The range accuracy σ_m depends on the sensors. The distance between scan lines varies because it depends on the vehicle speed. Thus λ_t should be large enough to avoid the gap and meanwhile

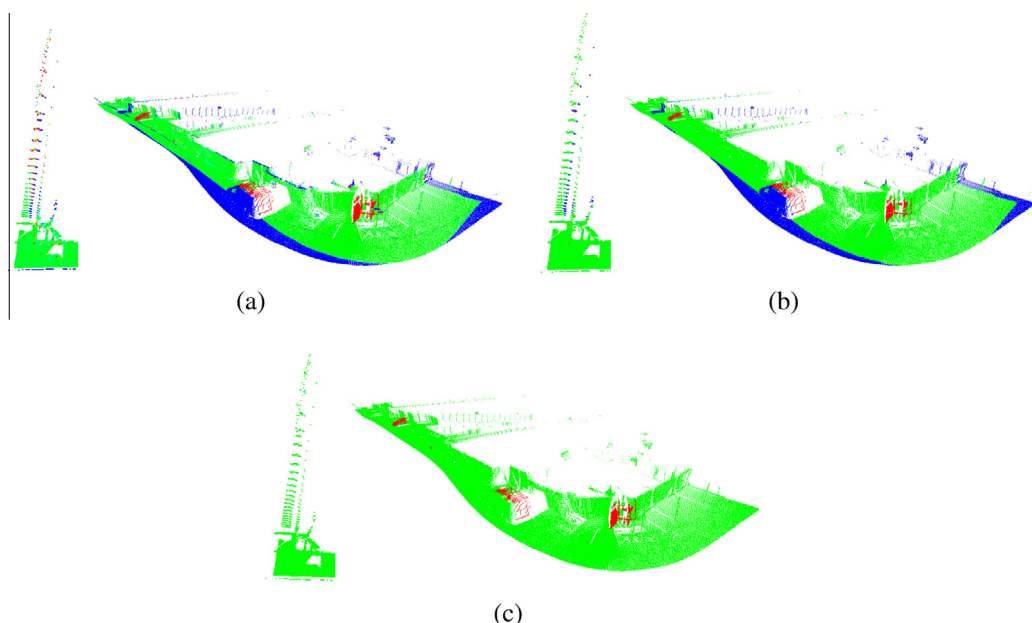


Fig. 8. Change detection result of Data 1 with 301,903 points. (a) occupancy-based result (changes in red); (b) improved by considering point normals. Especially in the enlarged part (on the left), ground points that are far from the laser center are rectified (green in (b), red in (a)); (c) hand labelled ground truth. (For interpretation of the references to color in this figure legend, the reader is referred to the web version of this article.)

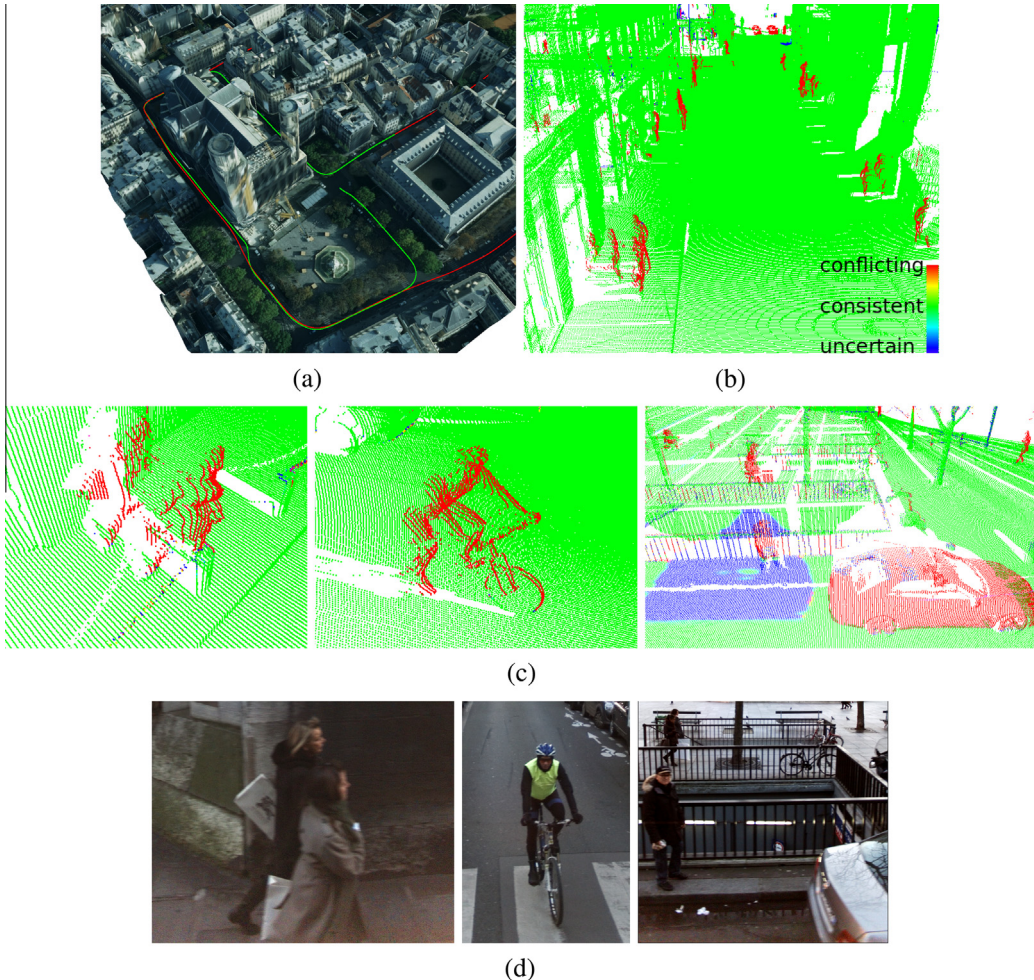


Fig. 9. Study site and some change detection examples. (a) trajectories of two epoch datasets in red and green around a cathedral; (b) one site of detected changes (red); (c) successfully detected pedestrians that are close to façade and bollards, a cyclist and a car and the shadow (blue) of another car in the reference data. Notice the correctly detected pedestrian in the middle of the shadow; (d) corresponding images (the laser scanner and cameras have different points of view). (For interpretation of the references to color in this figure legend, the reader is referred to the web version of this article.)

not too large either. The average distance between scan lines is about 0.1 m. λ_s depends on λ_o which covers the gaps along the rotating plane, therefore it should be larger than half of the angular resolution. λ_n defines the occupancy scope in the normal direction. It should be bigger than the registration error ($\sigma_r = 0.1$ m), however not too big to avoid over-modelling. Based on experimental results, it is set as 0.3 m.

If the time span is large between two epochs, changes may be found on buildings or street facilities which is useful for database updating. If the time span is short, e.g. two epochs scanned in the same day, most changes are caused by moving objects such as cars or pedestrians which is also important because these movable objects need not to be modelled or stored in a database. Data with clean street environment is of great importance for street inventory and especially mobility assessment. Movable objects may be considered as obstacles if they are located on pavements (Serna and Marcotegui, 2013).

Partial results of the first dataset (Data 1) using occupancy-based and PTTD-based methods are presented in our previous work (Xiao et al., 2013), in which many urban objects, e.g. garbage bins, chairs, motorcycles, are illustrated. Fig. 8 shows the comparison with the improved occupancy-based method by considering point normals. Previous method performs weak for the points whose normal direction are extremely different from the directions of their rays, e.g. ground points that are far from the laser center. Fig. 9 depicts the study site of Data 2 and some

detected movable objects, e.g. pedestrians, bicycles and cars, using the occupancy and PTTD combined method.

Fig. 10 illustrates the results of a large area using different methods. The occupancy-based method successfully differentiates points that are occluded or have no neighboring rays with real changed points. Occluded points are detected as *uncertain* (blue), and unchanged points are *consistent* (green), whereas changed points are *conflicting* (red) with reference data. Many points on the ground that are far from the laser center are falsely detected as changed (Fig. 10b) using previous occupancy-based method. There are rectified by considering point normals (Fig. 10c). However, many points on trees and fences are detected as *conflicting*. The PTTD-based method is also able to detect all the changes (Fig. 10d). It has better performance for penetrable objects, because neighboring triangles can be found from the reference data. However, all points in shadows are incorrectly detected as changed. The integrated approach combines the advantages of both (Fig. 10e). Occlusion changes are distinguished from real changes and false detections on penetrable objects are excluded. Notice that there are many false detections on trees in Fig. 10c and d, whereas much less in Fig. 10e. This is because only points that are both conflicting with reference rays and far from nearest triangles are detected as changed. Fig. 10f shows the manually labelled ground truth. Some points on a fast moving object on the street have not been labelled due to the irregular structure. However they are correctly detected.

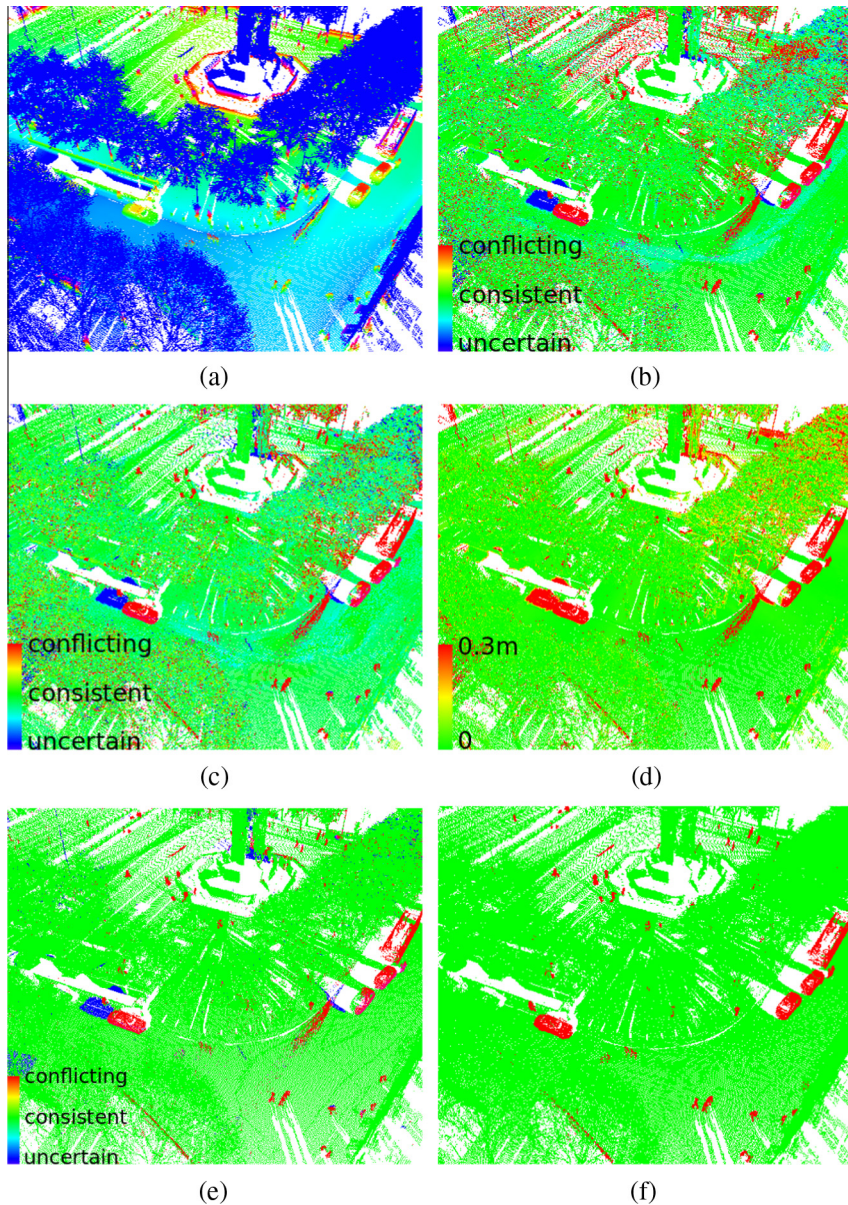


Fig. 10. Change detection results by different methods. (a) original data colored by height; (b) occupancy-based method: occluded points (blue) are distinguished from real changed points (red), many points on the ground are incorrectly detected as changed; (c) occupancy-based method with point normals: some points on trees are still incorrectly detected as changed; (d) PTTD-based method: occluded and real changed points are both detected as changed (red); (e) combination method: real changes are differentiated from occlusions, incorrectly detected points on trees are excluded; (f) manually labelled ground truth (changes in red). (For interpretation of the references to color in this figure legend, the reader is referred to the web version of this article.)

Table 2
Accuracy assessment of methods using PTTD, occupancy, occupancy with point normals (Occ + Norm) and its combination with PTTD (the greatest value of each column is in bold).

Method	Data 1				Data 2			
	R	P	JC	F_1	R	P	JC	F_1
PTTD	0.917	0.105	0.104	0.189	0.865	0.277	0.265	0.419
Occ – Norm	0.987	0.760	0.753	0.859	0.902	0.363	0.349	0.517
Occ + Norm	0.963	0.875	0.846	0.917	0.876	0.467	0.438	0.609
Combined	0.907	0.946	0.862	0.926	0.812	0.857	0.715	0.834

6. Evaluation and discussion

Since our method detects changes for each point, the accuracy is firstly assessed at point level. Ground truth has been labelled

manually. Four methods, i.e. PTTD-based method, occupancy-based method without point normals (Occ – Norm), occupancy-based method with point normals (Occ + Norm) and its combination with PTTD-based method (Combined =

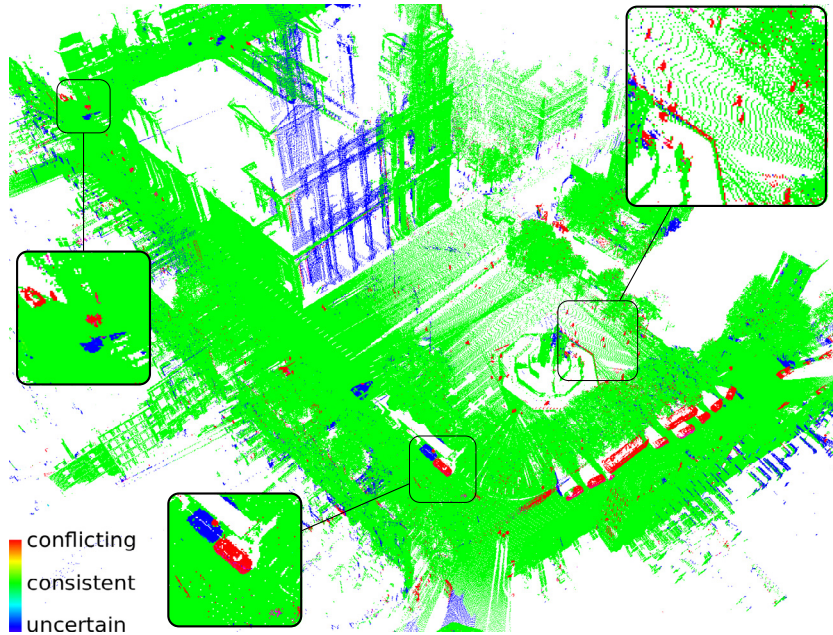


Fig. 11. Street environment change detection result of the combination of occupancy-based and PTTD-based methods: real changes are differentiated from occlusions, incorrectly detected points on trees are excluded (data sub-sampled due to huge size).

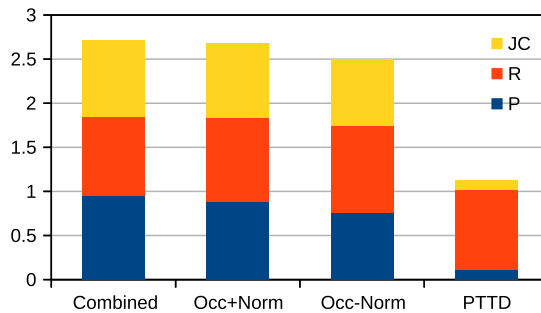


Fig. 12. Change detection results of Data 1 using different methods. PTTD-based method performs the worst due to occlusions. Considering point normals improves the occupancy-based method. The combined method performs the best.

PTTD + Occ + Norm), are evaluated against the ground truth. True positive (TP) is the number of changed points correctly detected. False positive (FP) is the number of unchanged points that are detected as changed. False negative (FN) is the number of changed

points detected as unchanged. True negative (TN) is the number of unchanged points correctly detected. The majority of the points are unchanged and more than 97.8% of the whole dataset are correctly detected as unchanged, so it is unnecessary to quantify TN rate and the overall accuracy (including TN). Recall (R), precision (P), Jaccard coefficient (JC) (Radke et al., 2005) and F_1 score are quantified. Evaluation results of the two data are given in Table 2.

$$\begin{aligned} R &= TP/(TP + FN) \\ P &= TP/(TP + FP) \\ JC &= TP/(TP + FN + FP) \\ F_1 &= 2 \cdot P \cdot R/(P + R) \end{aligned} \quad (12)$$

The two datasets give similar results. The occupancy-based method shows highest recall, and the combined method dominates all the other values. In general, the values are higher for Data 1 than for Data 2, because Data 1 is simpler and smaller. Especially, the occupancy-based method has much higher precision in Data 1 than Data 2 because there are less penetrable objects. The improved occupancy-based method (Occ + Norm) significantly increases the

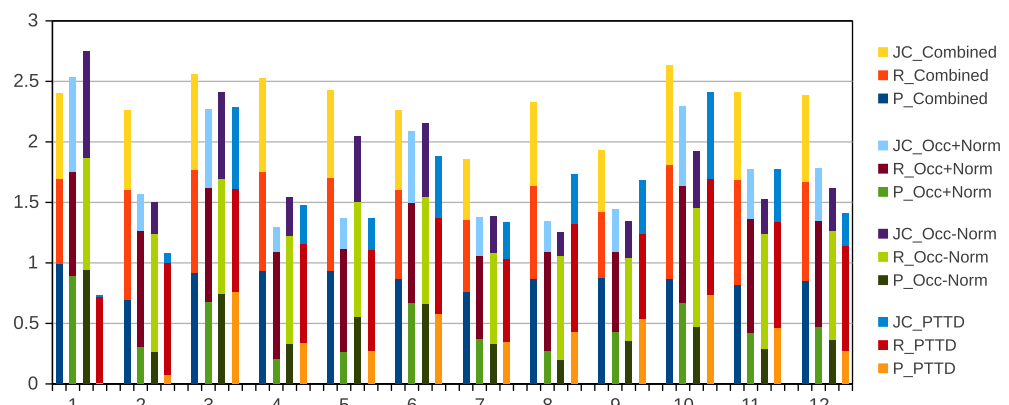


Fig. 13. Change detection results of Data 2. Number 1–11 are the 11 subsets, number 12 is the whole dataset. Results of subsets vary according to different scenes. Result of the whole dataset is consistent with Data 1.

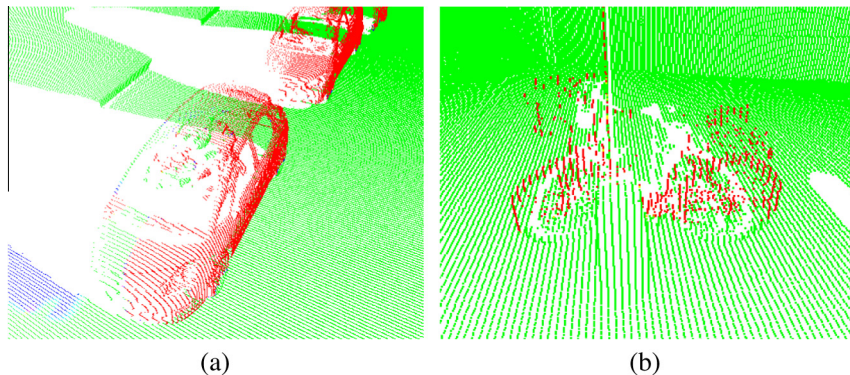


Fig. 14. Examples of false detections. (a) A car has been partially detected as changed whereas the other part as unchanged because this part is overlapped with another car in the reference data; (b) a bicycle is leaning against a pole and the majority part of it is correctly detected, however the very lower parts of the wheels are misdetected as unchanged; few points on the pole are also misdetected as changed.

precision, however decreases the recall, which can be caused by normal estimation errors. Both occupancy-based and PTTD-based methods give a low level of precision, especially for Data 2. However the reasons are different. For the occupancy-based method, errors come from the points on penetrable objects. As depicted in Fig. 10c, there is a large number of falsely detected tree points. For the PTTD-based method, it is due to occlusion. As shown in Fig. 11, a big part of the façade (blue) is occluded. Therefore, the combination of them avoids these drawbacks resulting in a high level of precision. The recall of combined method is smaller than the others because points need to meet both the criteria as mentioned in the previous section.

Fig. 12 illustrates the add-up of precision, recall and JC values. It is clear that occupancy-based method is improved by considering point normals. And the combination with PTTD helps to further improve the final result. Fig. 13 shows the results of each subset of Data 2 (number 1–11) and the whole dataset (number 12). Due to large amount of data, the laser scanner automatically stores acquired points into different files. Each subset corresponds to one file and contains three million points. Subsets 1–7 are acquired behind and beside the cathedral in Fig. 9a) and there are barely penetrable objects on the narrow streets as shown in Fig. 9(b). Whereas the others contain many points on trees that are in the front of the cathedral, such as in Fig. 10. The results varies due to different street scenes. In general, occupancy-based results are better than PTTD-based when there are few penetrable objects (subsets 1–7), and vice versa. Considering point normals improves the occupancy-based results when point normals differ from their ray directions (subsets 2, 8, 9, 10, 11), however it also hinders the results to some extent depending on the normal estimation accuracy (subsets 1, 3, 4, 5, 6). The combined method has the best results for all the subsets except the first one, because the PTTD-based result is extremely bad. The overall result (dataset 12) shows the same pattern as in Fig. 12, meaning the combined method performs the best in a complex urban street environment. However, individual methods have strengths at certain street scenes.

Failure of detection is caused by (i) object replaced by another: the object has changed but locates at the same location as a previous one (Fig. 14a); (ii) object points are near the ground: points on the ground give evidence of consistency to nearby points and are also within the PTTD threshold (Fig. 14b); (iii) noise: some points presented in the data are too sparse to represent meaningful street objects, e.g. objects that are too far from the laser scanner.

To evaluate the accuracy at object level, we consider an object as detected if a large portion (90%) of its points are correctly detected. In Data 1, three changed objects, a pedestrian, a van

and a car, are all correctly detected. In Data 2, a total of 229 objects are observed in the target dataset. All of these objects are successfully detected except one (Fig. 14a), which is partially detected (lower than 90%) because another object from the reference dataset is located at the same space. No unchanged objects are incorrectly detected. Most of the falsely detected changed points are sparsely distributed so that they can be treated as noise in the following process. For instance, after clustering all the changed points into objects, those objects with a small number of points can be eliminated.

7. Conclusions

A general framework for change detection in urban street environments was presented. The method combines both advantages of occupancy grids from robotics and conventional distance-based methods. The former indicates occluded areas thus helps to distinguish occlusions and points without counterparts from real changes. The latter is robust to penetrable objects which are self-conflicting in terms of occupancy. They are complementary to each other.

The occupancy-based method is based on the physical laser scanning mechanism. The prerequisite is to know the origin of each scanned point. A local cylindrical reference frame is built for each ray and its point. Then the occupancy of space is modelled around the ray and the point. Gaps between rays are interpolated by treating the ray shape as a triangular prism instead of a cone. Thus it is robust to irregular point density. Point normals are considered to improve the occupancy modelling around the point and its surface. Changes are detected directly at point level without voxelization. A distance-based method, PTTD is chosen to optimize the occupancy-based result. PTTD keeps the flexibility to be suitable to complex street objects, and also the robustness to irregular point distributions. Urban object changes are automatically detected at point level in complex street environments.

The limitation of the proposed method is that objects replaced by another can not be detected. Future work will focus on fine scale feature-based change detection.

Acknowledgements

This study has been performed as part of the Cap Digital Business Cluster TerraMobilita Project. The authors would like to thank TerraMobilita project members for the comments, the Stereopolis team for data acquisition, and the anonymous reviewers for their constructive suggestions.

References

- Aijazi, A.K., Checchin, P., Trassoudaine, L., 2013. Detecting and updating changes in lidar point clouds for automatic 3d urban cartography. In: ISPRS Annals of Photogrammetry, Remote Sensing and Spatial Information Sciences, vol. II-5/W2, pp. 7–12.
- Banno, A., Masuda, T., Oishi, T., Ikeuchi, K., 2008. Flying laser range sensor for large-scale site-modeling and its applications in bayon digital archival project. *Int. J. Comput. Vision* 78 (2–3), 207–222.
- Champion, N., Rottensteiner, F., Matikainen, L., Liang, X., Hyppä, J., Olsen, B., 2009. A test of automatic building change detection approaches. In: International Archives of the Photogrammetry, Remote Sensing and Spatial Information Sciences, vol. XXXVIII-3/W4, pp. 145–150.
- Chauve, A.-L., Labatut, P., Pons, J.-P., 2010. Robust piecewise-planar 3d reconstruction and completion from large-scale unstructured point data. In: IEEE Conference on Computer Vision and Pattern Recognition (CVPR), pp. 1261–1268.
- Choi, K., Lee, I., Kim, S., 2009. A feature based approach to automatic change detection from lidar data in urban areas. In: International Archives of the Photogrammetry, Remote Sensing and Spatial Information Sciences, vol. XXXVIII, pp. 259–264.
- Demantké, J., Mallet, C., David, N., Vallet, B., 2011. Dimensionality based scale selection in 3d lidar point clouds. In: International Archives of the Photogrammetry, Remote Sensing and Spatial Information Sciences, vol. XXXVIII-5/W12, pp. 97–102.
- Eden, I., Cooper, D.B., 2008. Using 3d line segments for robust and efficient change detection from multiple noisy images. In: European Conference on Computer Vision (ECCV), pp. 172–185.
- Frih, C., Zakhori, A., 2004. An automated method for large-scale, ground-based city model acquisition. *Int. J. Comput. Vision* 60 (1), 5–24.
- Girardeau-Montaut, D., Roux, M., Marc, R., Thibault, G., 2005. Change detection on points cloud data acquired with a ground laser scanner. In: International Archives of the Photogrammetry, Remote Sensing and Spatial Information Sciences, vol. 36, pp. 30–35.
- Greene, N., 1994. Detecting intersection of a rectangular solid and a convex polyhedron. In: Graphics Gems IV. Elsevier, pp. 74–82.
- Hebel, M., Arens, M., Stilla, U., 2013. Change detection in urban areas by object-based analysis and on-the-fly comparison of multi-view als data. *ISPRS J. Photogramm. Rem. Sens.* 86, 52–64.
- Hussain, M., Chen, D., Cheng, A., Wei, H., Stanley, D., 2013. Change detection from remotely sensed images: from pixel-based to object-based approaches. *ISPRS J. Photogramm. Rem. Sens.* 80, 91–106.
- Irani, M., Anandan, P., 1998. A unified approach to moving object detection in 2d and 3d scenes. *IEEE Trans. Pattern Anal. Mach. Intell.* 20 (6), 577–589.
- Kang, Z., Zhang, L., Yue, H., Lindenbergh, R., 2013. Range image techniques for fast detection and quantification of changes in repeatedly scanned buildings. *Photogramm. Eng. Rem. Sens.* 79 (8), 695–707.
- Košecka, J., 2013. Detecting changes in images of street scenes. In: Asian Conference on Computer Vision (ACCV), pp. 590–601.
- Lafarge, F., Mallet, C., 2011. Building large urban environments from unstructured point data. In: IEEE International Conference on Computer Vision (ICCV), pp. 1068–1075.
- Lindstrom, M., Eklundh, J., 2001. Detecting and tracking moving objects from a mobile platform using a laser range scanner. In: International Conference on Intelligent Robots and Systems (IROS), vol. 3, pp. 1364–1369.
- Matikainen, L., Hyppä, J., Hyppä, H., 2003. Automatic detection of buildings from laser scanner data for map updating. In: International Archives of the Photogrammetry, Remote Sensing and Spatial Information Sciences, vol. 34-3/W13, pp. 218–224.
- Monnier, F., Vallet, B., Soheilian, B., 2012. Trees detection from laser point clouds acquired in dense urban areas by a mobile mapping system. In: ISPRS Annals of Photogrammetry, Remote Sensing and Spatial Information Sciences, vol. I-3, pp. 245–250.
- Monnier, F., Vallet, B., Paparoditis, N., Papelard, J.-P., David, N., 2013. Registration of terrestrial mobile laser data on 2d or 3d geographic database by use of a non-rigid icp approach. In: ISPRS Annals of Photogrammetry, Remote Sensing and Spatial Information Sciences, vol. II-5/W2, pp. 193–198.
- Moras, J., Cherfaoui, V., Bonnifait, P., 2011. Credibilist occupancy grids for vehicle perception in dynamic environments. In: IEEE International Conference on Robotics and Automation (ICRA). IEEE, pp. 84–89.
- Murakami, H., Nakagawa, K., Hasegawa, H., Shibata, T., Iwanami, E., 1999. Change detection of buildings using an airborne laser scanner. *ISPRS J. Photogramm. Rem. Sens.* 54 (2), 148–152.
- O'Callaghan, R., Haga, T., 2007. Robust change-detection by normalised gradient-correlation. In: IEEE Conference on Computer Vision and Pattern Recognition (CVPR), pp. 1–8.
- Pagac, D., Nebot, E., Durrant-Whyte, H., 1996. An evidential approach to probabilistic map-building. In: IEEE International Conference on Robotics and Automation (ICRA), vol. 1, pp. 745–750.
- Paparoditis, N., Papelard, J., Cannelle, B., Devaux, A., Soheilian, B., David, N., Houzay, E., 2012. Stereopolis ii: a multi-purpose and multi-sensor 3d mobile mapping system for street visualisation and 3d metrology. *Revue Française de Photogrammétrie et de Télédétection* 200, 69–79.
- Pollard, T., Mundy, J.L., 2007. Change detection in a 3-d world. In: IEEE Conference on Computer Vision and Pattern Recognition (CVPR), pp. 1–6.
- Poullis, C., 2013. A framework for automatic modeling from point cloud data. *IEEE Trans. Pattern Anal. Mach. Intell.* 35, 2563–2575.
- Pu, S., Rutzinger, M., Vosselman, G., Oude Elberink, S., 2011. Recognizing basic structures from mobile laser scanning data for road inventory studies. *ISPRS J. Photogramm. Rem. Sens.* 66 (6), S28–S39.
- Qin, R., Gruen, A., 2014. 3d change detection at street level using mobile laser scanning point clouds and terrestrial images. *ISPRS J. Photogramm. Rem. Sens.* 90, 23–35.
- Radke, R.J., Andra, S., Al-Kofahi, O., Roysam, B., 2005. Image change detection algorithms: a systematic survey. *IEEE Trans. Image Process.* 14 (3), 294–307.
- Rutzinger, M., Ruf, B., Höfle, B., Vetter, M., 2010. Change detection of building footprints from airborne laser scanning acquired in short time intervals. In: International Archives of the Photogrammetry, Remote Sensing and Spatial Information Sciences, vol. XXXVIII, pp. 475–480.
- Sakurada, K., Okatani, T., Deguchi, K., 2013. Detecting changes in 3d structure of a scene from multi-view images captured by a vehicle-mounted camera. In: IEEE Conference on Computer Vision and Pattern Recognition (CVR), pp. 137–144.
- Serna, A., Marcotegui, B., 2013. Urban accessibility diagnosis from mobile laser scanning data. *ISPRS J. Photogramm. Rem. Sens.* 84, 23–32.
- Serna, A., Marcotegui, B., 2014. Detection, segmentation and classification of 3d urban objects using mathematical morphology and supervised learning. *ISPRS J. Photogramm. Rem. Sens.* 93, 243–255.
- Steinle, E., Bahr, H., 2003. Detectability of urban changes from airborne laser scanning data. In: International Archives of the Photogrammetry, Remote Sensing and Spatial Information Sciences, vol. 34-7/B, pp. 1135–1140.
- Taneja, A., Ballan, L., Pollefeys, M., 2011. Image based detection of geometric changes in urban environments. In: IEEE International Conference on Computer Vision (ICCV), pp. 2336–2343.
- Taneja, A., Ballan, L., Pollefeys, M., 2013. City-scale change detection in cadastral 3d models using images. In: IEEE Conference on Computer Vision and Pattern Recognition (CVPR), pp. 113–120.
- Tian, J., Reinartz, P., d'Angelo, P., Ehlers, M., 2013. Region-based automatic building and forest change detection on cartosat-1 stereo imagery. *ISPRS J. Photogramm. Rem. Sens.* 79, 226–239.
- Toshev, A., Mordohai, P., Taskar, B., 2010. Detecting and parsing architecture at city scale from range data. In: IEEE Conference on Computer Vision and Pattern Recognition (CVPR), pp. 398–405.
- Ulusoy, A.O., Mundy, J.L., 2014. Image-based 4-d reconstruction using 3-d change detection. In: European Conference on Computer Vision (ECCV), pp. 31–45.
- Underwood, J.P., Gillsjo, D., Bailey, T., Vlaskine, V., 2013. Explicit 3d change detection using ray-tracing in spherical coordinates. In: IEEE International Conference on Robotics and Automation (ICRA), pp. 4735–4741.
- Verma, V., Kumar, R., Hsu, S., 2006. 3d building detection and modeling from aerial lidar data. In: IEEE Conference on Computer Vision and Pattern Recognition (CVPR), vol. 2, pp. 2213–2220.
- Vögtle, T., Steinle, E., 2004. Detection and recognition of changes in building geometry derived from multitemporal laserscanning data. *Int. Arch. Photogramm. Rem. Sens. Spatial Inform. Sci.* 35 (B2), 428–433.
- Vosselman, G., Gorte, B., Sithole, G., 2004. Change detection for updating medium scale maps using laser altimetry. In: International Archives of the Photogrammetry, Remote Sensing and Spatial Information Sciences, vol. 34/B3, pp. 12–23.
- Walter, V., 2004. Object-based evaluation of lidar and multispectral data for automatic change detection in gis databases. In: International Archives of the Photogrammetry, Remote Sensing and Spatial Information Sciences, vol. 35, pp. 723–728.
- Weinmann, M., Jutzi, B., Mallet, C., 2014. Semantic 3d scene interpretation: a framework combining optimal neighborhood size selection with relevant features. In: ISPRS Annals of Photogrammetry, Remote Sensing and Spatial Information Sciences, vol. II-3, pp. 181–188.
- Wolf, D., Sukhatme, G.S., 2004. Online simultaneous localization and mapping in dynamic environments. In: IEEE International Conference on Robotics and Automation (ICRA), vol. 2, pp. 1301–1307.
- Xiao, W., Vallet, B., Paparoditis, N., 2013. Change detection in 3d point clouds acquired by a mobile mapping system. In: ISPRS Annals of Photogrammetry, Remote Sensing and Spatial Information Sciences, vol. II-5/W2, pp. 331–336.
- Xu, S., Vosselman, G., Oude Elberink, S., 2013. Detection and classification of changes in buildings from airborne laser scanning data. In: ISPRS Annals of Photogrammetry, Remote Sensing and Spatial Information Sciences, vol. II-5/W2, pp. 343–348.
- Yang, B., Dong, Z., 2013. A shape-based segmentation method for mobile laser scanning point clouds. *ISPRS J. Photogramm. Rem. Sens.* 81, 19–30.
- Yin, Z., Collins, R., 2007. Belief propagation in a 3d spatio-temporal mrft for moving object detection. In: IEEE Conference on Computer Vision and Pattern Recognition (CVPR), pp. 1–8.
- Yu, X., Hyppä, J., Kaartinen, H., Maltamo, M., 2004. Automatic detection of harvested trees and determination of forest growth using airborne laser scanning. *Rem. Sens. Environ.* 90 (4), 451–462.
- Zeibak, R., Filin, S., 2007. Change detection via terrestrial laser scanning. In: International Archives of the Photogrammetry, Remote Sensing and Spatial Information Sciences, vol. 36-3/W52, pp. 430–435.
- Zhou, Q.-Y., Neumann, U., 2010. 2.5d dual contouring: A robust approach to creating building models from aerial lidar point clouds. In: European Conference on Computer Vision (ECCV), pp. 115–128.
- Zhou, L., Vosselman, G., 2012. Mapping curbstones in airborne and mobile laser scanning data. *Int. J. Appl. Earth Obs. Geoinf.* 18, 293–304.